Verdú Amat, S.; Barat Baviera, JM.; Grau Meló, R. (2019). Fresh-sliced tissue inspection: Characterization of pork and salmon composition based on fractal analytics. Food and Bioproducts Processing. 116:20-29. https://doi.org/10.1016/j.fbp.2019.04.008

**Fresh-sliced tissues inspecting: characterization of pork and salmon composition based on fractal analytics**

Samuel Verdú, José M. Barat, Raúl Grau.

Departamento de Tecnología de Alimentos. Universidad Politècnica de València, Spain.

*Author for correspondence: Samuel Verdú

**Address:** Edificio 8G - Acceso F – Planta 0

Ciudad Politécnica de la Innovación

Universidad Politécnica de Valencia

Camino de Vera, s/n

46022 VALENCIA – SPAIN

**E-mail:** saveram@upvnet.upv.es

**Abstract**

The capability of fractal analytics of digital images for characterizing fresh sliced tissues from different nature (pork-loin and salmon) was tested. Characterization was focused to determinate the fat and water fraction of samples, and how affect the idiosyncrasy of tissues morphology in this aim. It was carried out extracting fractal information based on two pre-stablished parameters (fractal dimension and lacunarity) from different type of pre-processed images based on color scale and channel (*grayscale* and *RGB*). Thus, relationship of evolution of fractal parameters across tones with morphology of tissues was studied by means of the resulting spectra. All information was divided in two data blocks: the first one was the composition features (fat and water fraction) and the second one the fractal information generate from fractal parameters and image type combinations, which was treated as multivariable data matrix. Finally, the dependency of the two data blocks was tested using multivariate nonlinear regression assays. The results report a high dependency of fractal information to fat and water fraction for both pork-loin and salmon. The two fractal parameters and all image types reported satisfactory results excepting blue channel (*B*) for salmon, which present reduced dependency compared with the rest. Fractal analytics of images proved its capacity to be a simple and rapid non-destructive technique for characterizing the composition of tissues from different nature and complexity, which could complement processes of inspection with the aim of improve classification and selection operations within production chain.

**Keywords:** fresh sliced tissues, inspection, fractal analytics, image, characterization, composition

## 1. Introduction

The necessity of yield increments in industrial processes in addition of sophistication for the implied operations within production chains, concretely for food industry, generates requirements of new developments which keep the system under control at the same time of the costs are reduced to minimum. When a concrete food sector requires exceptional control measures of hygienic parameters, such as which that produce fresh and raw materials (meat, fish, dairy, etc.), the development of fast and simple non-destructive inspection techniques provide notable advantages to the entire production system.

The main advantage is the increase of velocity in a given operation, and then a high rate of samples analysed could be reached per unit of time, allowing collect information from entire lots, sample by sample. The fact of obtaining information in continuous way from each sample allows increase the accuracy in inspection operations, improving later automatic works as classification, slicing, packaging, labelling, storage, etc. In this sense, one of the most productive areas within the non-destructive fresh products control and monitoring has been the image analysis in several categories. Some of these categories are visible image in 2D, spectral imaging, X-ray imaging among others. Applications such as the classification of pork hams, assessing of beef carcasses tenderness, the freshness control of gilthead sea bream based on gill and eye color changes, the automatic fishbone detection, etc. (Dowlati et al., 2013; Ivorra, Verdu, Sánchez, Grau, & Barat, 2016; Jackman, Sun, & Elmasry, 2012; Konda Naganathan et al., 2015; Mery et al., 2011) have been reported previously, proving the potential of those group of technologies destined to this aim. Visible image analysis is one of the

most accessible techniques, from which a wide number of studies has been reported having successful results in diverse research area in relation to the versatility and reduced cost possibilities. Into this technique is included fractal analysis of digital images.

Fractal analysis is a group of calculate algorithms used to study and characterizing systems with high complexity and chaotic structures, with the aim of detect measurable patterns which could offer valuable information from a given sample. An example of those types of systems is the biological structures. Concretely biological systems have been largely studied using fractal analytics of digital images within biomedical and histological research areas, reporting useful applications for characterizing and diagnosis of organic structure features. Some of these applications have been applied to study neurophysiology systems, organ malformations or glucose fluctuation kinetics among others (Akar, Kara, Akdemir, & Kiriş, 2015; Kesić & Spasić, 2016; Weissman & Binah, 2014). Thus, the application of this technique to food industry presents a real potential to be exploited. Some recent studies have been reported about the application of fractal analysis for characterising fresh food tissues from different nature and processing, both fresh meat and fish products. Influence of factors such the origin, freshness and processing of tissues are characterised and modelled successfully processing the fractal information. Some examples are the characterization of fatty infiltration in Iberian and White pork sirloins, color changes in the surface of fresh cut meat, the evaluation of the effects of frozen storage on the microstructure of tilapia (He, Zhu, Shen, Lin, & Xiao, 2015; Quevedo et al., 2013; Serrano, Perán, Jiménez-Hornero, & Gutiérrez de Ravé, 2013), as the evaluation of antioxidants in juices, bruise in red bayberries, browning in avocado, acrylamide in biscuits, characterization of low-fat yogurts, etc. (Lu, Zheng, Hu, Lou, & Kong, 2011; Lu & Zheng, 2012; Quevedo,

Ronceros, Garcia, Lopéz, & Pedreschi, 2011; Torres, Amigo Rubio, & Ipsen, 2012; Zheng et al., 2011). Although these studies have shown the effectiveness of fractals, the main use of fractal analytics has been as a tool to classifying and characterizing, from qualitatively point of view, the composition of some products. The development of non-invasive tools focused to that aim, mainly with quantification capacity, is according to the tendency of recent food regulations, such as (UE) n.º 1169/2011 from European Parliament about food information supplied to consumers, which forces the food producer to include the nutritional labelling in the most of processed food products. Thus, the aim of this work was the evaluation of fractal analytics of digital images as a non-destructive inspecting tool of food fresh sliced tissues from different nature (pork-loin and salmon) focused to the quantification of the composition in terms of fat and water fraction.

## 2. Material and methods

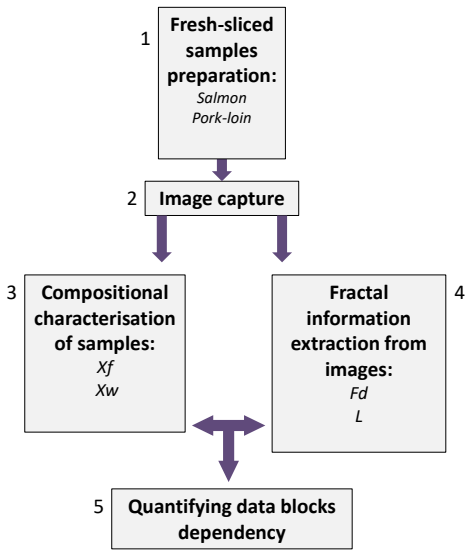


Figure 1. Experiment procedure scheme. *Xw*: water fractio; *Xf*: fat fraction; *R*, *G* and *B*: red, green and blue color image channels respectively; *Fd*: fractal dimension; *L*: lacunarity

### 2.1. Fresh-sliced samples preparation

Two types of fresh-sliced tissues from different nature were used: pork-loin and salmon. Both represent different-origin comestibles tissues which are commonly sliced, packaged and labeled automatically to be sold. Twenty six slices of fresh pork-loin from five different lots and twenty slices of fresh salmon from four different lots were bought in a local provider. All slices presented dimensions within 1±0.5 cm of thickness and 15±2.1 cm of length (Step 1 in Figure 1).

### 2.2 Image capture

Images were obtained using a standard device which could easily be implemented to on-line inspection within production chain. Single image of each slice were obtained through a HD webcam C615 (Logitech) fixed on a rigid structure leaving 20 cm of samples, and a LED lamp IP20 5W as lighting system. The camera was communicated to a laptop equipped with the control software. On the scene of the camera capture, a black matte material was placed to reduce reflections at the camera. Camera took images of 3264×2448 pixels with fine quality in JPEG format (Step 2 in Figure 1).

### 2.3 Compositional characterization of samples

Composition in terms of moisture fraction ($Xw$) and fat fraction ($Xf$), of both types of samples, were analyzed. Moisture was determined by oven drying to constant weight at 100 C (ISO Norm R-1442, 1979), and fat according to ISO Norm R-1443 (1973) using

a FOSS Soxtec System 2055 Tecator. All parameters were expressed in wet basis and analyzed by triplicate for each slice (Step 3 in Figure 1).

### 2.4. Image processing and fractal information extraction

With the aim of obtain a multivariable data matrixes of fractal information, images were processed following Zheng et al. (2011) method with modifications (Step 4 and 5 in Figure 1). The basic procedures were as follows:

1. Image of each sample was taken in *RGB* format and processed to several derived image types with the aim of simplifying information for processing. Formats were 8 bits *greyscale* and *RGB* splited color channels (red (*R*), green (*G*) and blue (*B*)). Then, 4 types of images were obtained from each sample.
2. Each image was thresholded and binaryzed for a tone value between 0 and 255. *Greyscale*: from maximum black (0) to maximum white (255); *R* channel: from maximum black (0) to maximum red (255), *G* channel: from maximum black (0) to maximum green (255), *B* channel: from maximum black (0) to maximum blue (255).
3. The two parameters fractal dimension (*Fd*) and lacunarity (*L*) were calculated for each thresholded image. Both fractal parameters consider in essence the relationship between the scale of a shape (box) used to scan the image and the number of this shape necessaries to complete the image (i.e. two box grids scale, Figure 2B and 2C). Fractal dimension (*Fd*) is based on box counting scan, where several grids of decreasing size (box scale) are disposed over different positions of an image and the number of boxes that contain pixels is counted for each grid size. Left part of Figure 2B and 2C (in loin sample as example) shows two

different box scales grids and the number of the box necessaries to complete all pixels from the thresholded image. Equation 1 represents *Fd* calculate:

$$Fd = -\lim_{n \to 0} \frac{log N\varepsilon}{log \varepsilon} \quad (1)$$

where *Fd* is fractal dimension, *Nε* is the number of boxes containing pixels at a given box scale and *ε* is the box scale. Then, *Fd* is the slope of the regression line for the log-log plot of box scale and box count. Left part of Figure 2D shows as look this type of plot, where determination coefficient was tested and equation of regression was calculated to obtain that slope absolute value.

In the other hand, Lacunarity (*L*) is based on quantifying the variation in pixel density at different box scale through lineal scanning across images. Right part of Figure 2B and 2C (in salmon sample as example) shows two different box scales grids and the start point and direction of the lineal scanning across entire thresholded image (black arrows). Scan was done from left to right, descending row by row once this was finished.

Equation 2 represents L calculate at each box scale:

$$L\varepsilon = \left(\frac{\sigma}{\mu}\right)^2 \quad (2)$$

where *Lε* is lacunarity at a given box scale, *σ* is standard deviation of pixels into boxes of that scale and *μ* is the average of pixels into boxes at that scale. Thus, *L* of entire is calculated as the average of values from all tested box sizes (right part of Figure 2D).

Both parameters were calculated in 15 different positions of grid for each image for avoid the effect of sample position within area of capture. Each one of the 15

result was taking as a single replica of each image. Data was obtained using FracLac for ImageJ created by Karperien (2013).

Finally, four spectra of each fractal parameter were obtained for each sample, from which a multivariate data block was made.

### 2.3 Quantifying of data block dependency

Dependency of compositional data (fat and water fraction) and multivariable fractal data blocks (fractal parameters spectra from *grayscale, R, G, B* and *RGB*) was tested by the nonlinear regression method Support Vector Machines (*SVM*). *SVM* are a powerful supervised learning methodology based on the statistical learning theory, which are commonly used for multivariable data analyses (Boser, Guyon, & Vapnik, 1992). Water and fat fractions dependencies of both the two fractal parameters spectra (*Fd* and *L*) and type of image information were tested with this method. Results were evaluated in terms of calibration (*Cal*) and crossvalidation (*CV*) coefficients following (Ropodi, Panagou, & Nychas, 2016), which suggest this procedure when the number of samples is either around or smaller than 40. Results were also evaluated by root mean square error (*RMSE*), which is a measure of the differences between values predicted by the model and the observed values that is being modelled. These individual differences are also called residuals, and the *RMSE* represent an aggregate of all them into a single measure.

$$RMSE = \sqrt{\frac{\Sigma_{i=1}^{n}(X_{o,i} - X_{m,i})^2}{n}}$$

where *Xo* is observed values and *Xm* is modelled values at place i. Procedures were performed with PLS Toolbox, 6.3 (Eigenvector Research Inc., Wenatchee, Washington, USA), a toolbox extension in the Matlab 7.6 computational environment (The Mathworks, Natick, Massachusetts, USA).

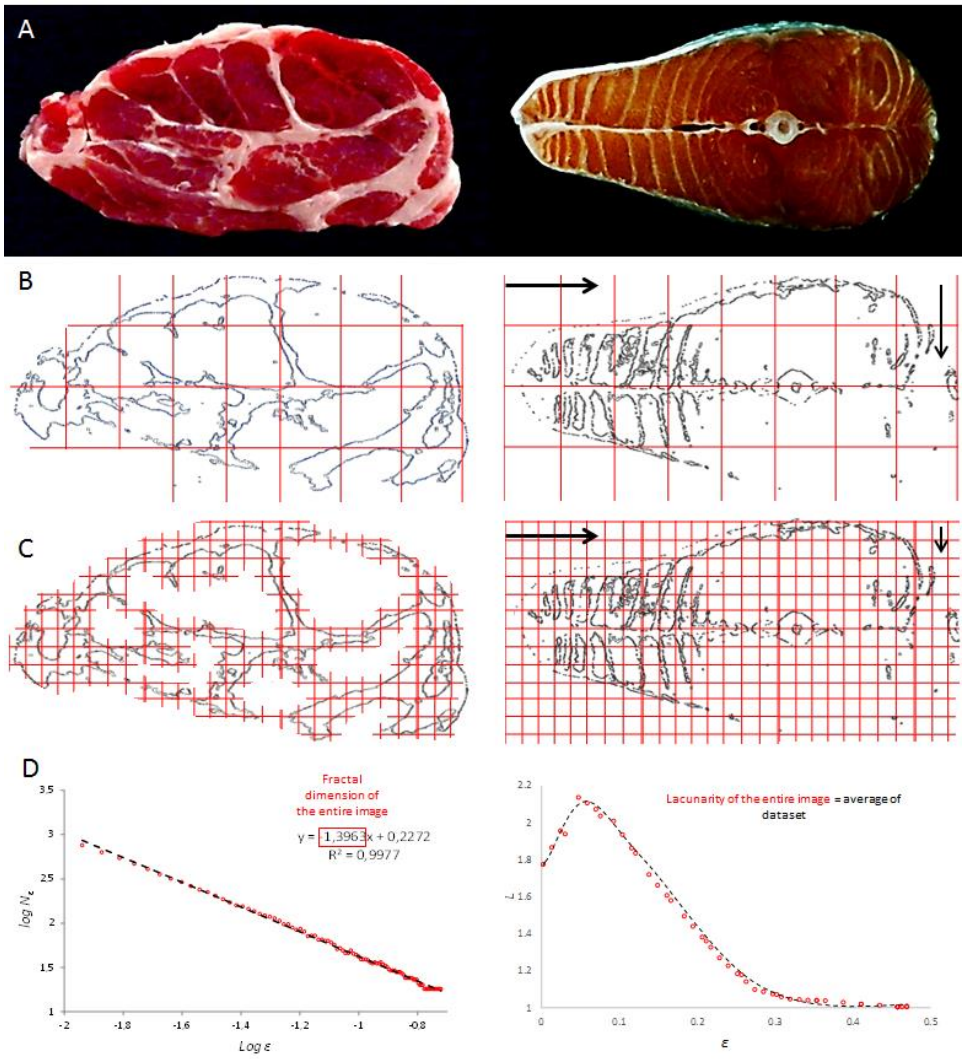


Figure 2. Scheme of fractal information obtaining. Left: Fractal dimendion (*Fd*); Right: Lacunarity (*L*). A: original taken images of a pork-loin and salmon samples; B: example of binary thresholded images with high box size grid. C: The same images with small box size grid. D: Performance plots and results of both fractal parameters; left: Fractal dimension is the slope of log *Nε* vs log *ε* plot (red square), where *Nε* is box count and ε

is the box scale; right: Lacunarity values from the image scan across box scale. Black arrows indicate start position and directionality of scan.

## 3. Results and discussion

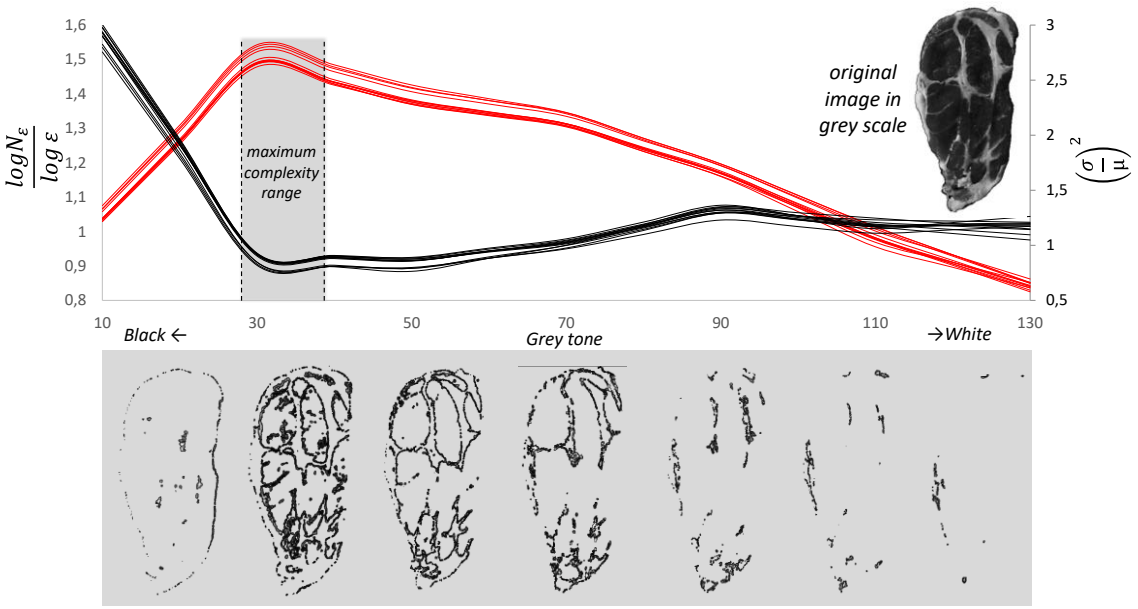


Figure 3. Example of evolution of fractal parameters Fractal dimension (*Fd*) and Lacunarity (*L*) across greyscale for a sample of pork-loin. Left axis represent Fractal dimension and right axis Lacunarity. Bottom zone correspond to obtained thresholded images follow graytones. Range between discontinued lines marks tones with images presenting maximum complex shape.

### 3.1 Fractal information extraction (Fd and L)

The relationship between fractal information variation and complexity of taken images was tested with the aim of observing the evidence of the influence by tissues components morphology. It is assumed that fractal information into spectra is meanly dependent of complexity of analyzed shapes because frequency of pixels in a given tone, but in this case it was ensured that a high charge of that the collected complexity into images came from the combination of the different components of sliced samples (fat and muscle tissues). Evolution of both fractal parameters across tones from each type of image were performed. Figure 3 shows the evolution of both fractal parameters across *grayscale* of a sample of pork-loin as example. Spectra denote a non-constant evolution across tones, forming peaks principally around tones 30-40. This behavior indicated a real variation following the tone, where inversed tendency between *Fd* and *L* was observed, although the main peak was produced in the same zone. Those peaks were function of type of image, observing variations compared to *R*, *G* and *B* spectra (Figure 5). Moreover, although both parameters were based in different calculate procedure, they reported equivalent information of complexity in this case.

In despite of proving the variability of fractal parameters, it was necessary attach the real processed images from which that dataset was obtained because an easy interpretation of spectra evolutions. Bottom zone of Figure 3 shows the evolution of processed images in *grayscale* of the pork-loin example. From tone 0 (black) it was observed an increment of complexity in images because a high number of pixels (frequency) in those tones, producing the maximum complexity just where fractal parameters generated the above commented peaks, from which complexity was reduced following the reduction of pixel number as it can be observed visually. Effectively, the shapes described by pixels in each tone correspond principally to variability in fat and

muscle tissues distributions taking as reference the original image one, therefore the most of complexity collected by images is due to this fact.

### 3.2 Results of data blocks dependency.

The relationship between tissues characteristics and fractal information was observed, however for a further characterization of samples, this variability needed being related to the amount of each tissue, fatty and lean, and then with the composition. Figure 4 shows an exploratory scatterplot representing *Fd* (left) and *L* (right) vs fat fraction (*Xf*) and water fraction (*Xw*) for all samples at tone 35 of grayscale, which was taken as average of the range tone within maximum complexity range across spectra (Figure 3). It can see how fractal parameters covariate with both *Xf* and *Xw* in inverse way, describing two distributions with marked tendencies but clear differences between pork-loin and salmon.

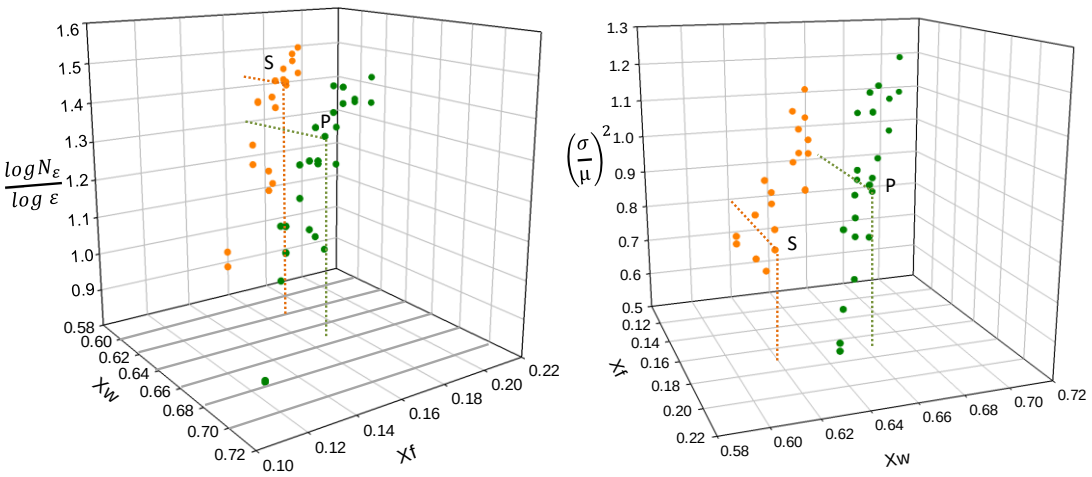


Figure 4. 3D scatterplot of *Fd* (left) and *L* (right) at tone 35 of *grayscale* (Z axis) vs. fat and water fraction (*Xf* and *Xw* respectively) from all samples of pork-loin (green dots)

and salmon (orange dots). Letters P and S marks an example of pork-loin and salmon samples respectively with a same amount of *Xf* but different fractal values.

*Fd* increased with fat fraction and decreased with water fraction. *L* present de inverse behavior such has been observed in the spectra of Figure 3. This phenomenon depends to the features of mathematical approach of both parameters. Although both had differences it was observed a high complementarity.

Distributions presented some differences in regard to type of sample. Sample types seemed have differences in their distributions, because salmon presented higher *Fd* values and lower L than pork-loin at a given fat fraction (points S and P in Figure 4). This feature could be explained because the differences in tissues morphology however, observing only one tone of *grayscale* was not enough to assume this fact. Thus, complete *Fd* spectra for grayscale, *R*, *G* and *B* channels from a sample of salmon and pork-loin with the same fat fraction (0.17±0.8) (points P and S at Figure 4) were plotted with the aim of exploring these behavior (Figure 5). Figure 5 shows the *Fd* spectra from salmon (orange) and pork-loin (green) in all image type. The first one was *grayscale* (Figure 5-A), which collects whole color variation transformed into grey tones. Spectra presented a maximum around tone 30-40 for the two types of sample. Until that zone, pork-loin present higher values than salmon according to scatterplot of Figure 4, however salmon presented higher values from tone 50 until the last one. That means the most part of scale. It was interpreted as salmon images presented higher complexity across light tones than pork-loin, which had instead high values at dark tones. This result was according to the fact that much of color of pork-loin was formed by intense red tonalities.

Although *greyscale* collects information from color features, spectra from each *RGB* channels could report more concrete information to characterizing samples. Figure 5B, C and D shows the spectra from *R*, *G* and *B* channels respectively. Spectra in *R* scale showed better the differences at dark tones of red, where pork-loin appeared with values of *Fd* quite higher than salmon. This behavior was inversed around tone 50, where salmon present high complexity at light tones again, as well as was observed in *grayscale*. *G* scale presented marked differences for salmon at light tones. In the same way for *B* scale, salmon had high values at light tones; however pork-loin presented the maximums values across the most of spectrum towards dark tones. Predominant colors of salmon was orange tones, which is formed by combinations of red and green tones principally, that explains the high values in light tones of *G* and an important part of *R* spectrum. On the other hand, the accentuated complexity of pork-loin in regard to dark tones of *R* and *B* channels is also explained because blue and red tones combination produced intense red-magenta colors, typical on this type of meat tissues. Overview, although all *RGB* channels presented variability in function of type of tissue, *R* appeared to collect the most influent information comparing with *grayscale*, reporting finally a high complexity for the salmon morphology across a high number of tones even having the same fat fraction.

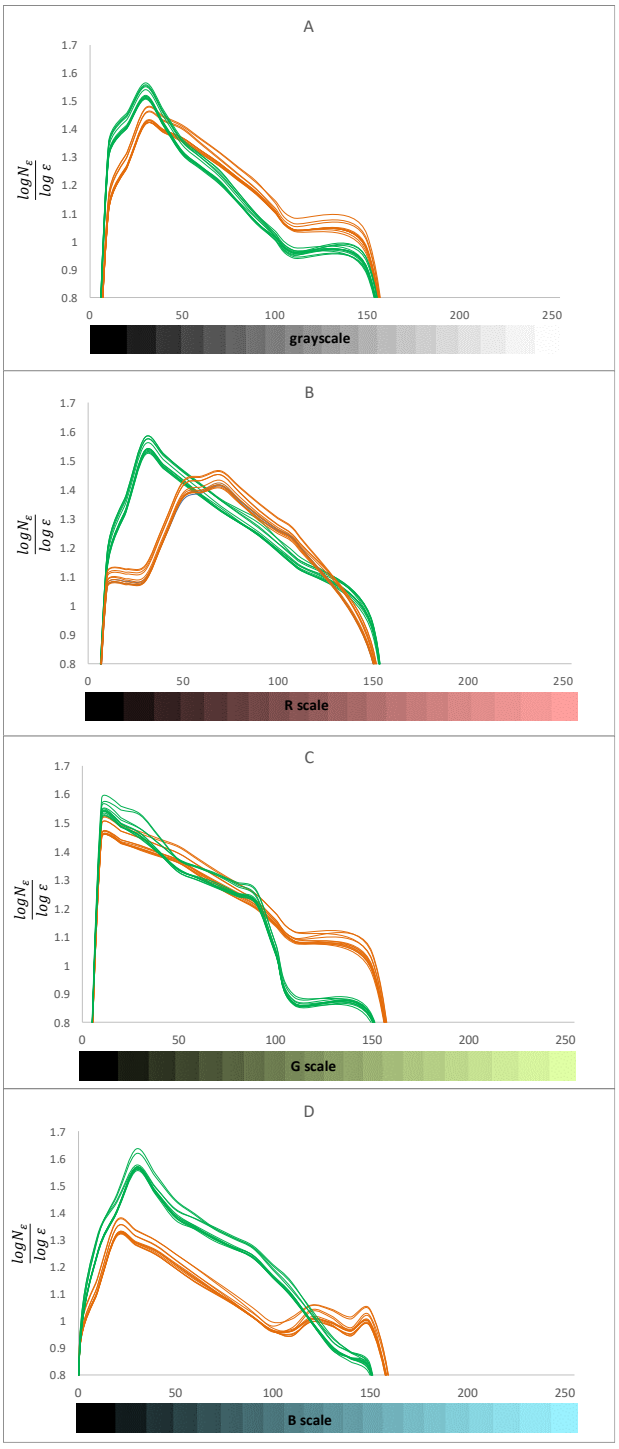


Figure 5. Spectra of *Fd* across *grayscale*, *R*, *G* and *B* channels from samples of pork-loin (green) and salmon (orange) with the same fat fraction. Raw spectra from each of 15 positions of grid into the each image were included. A: *Fd* spectra of grescale; B: *Fd* spectra of red scale; C: *Fd* spectra of green scale; D: *Fd* scale of blue scale.

Reported the capacity of fractal information to characterizing tissues from different nature, in regard to the relationship with composition and also morphology, the last step was to study and quantify the dependency of fractal information to fat and water fraction with the aim of developing a plausible quantifier application. Study was done taking as multivariable data block the spectra of *Fd* and *L* from each image type and channel: *grayscale*, *R*, *G* and *B*, and in addition *RGB* as an single block. The results of the nonlinear regressions carried out for each data block combination were collected into Table 1.

Results reported elevated coefficients for the most of combination data blocks for both calibration and cross-validation. Differences between *Xf* and *Xw* was not observed, both parameters presented high coefficients in regard to the two fractal parameters. About type of image and channel, all had coefficients up to 0.95, excepting the case of channel *B* for salmon, which presented 0.85 as maximum and 0.63 as minimum. Separated color channels showed a slight reduction in coefficients in general, trending to reach high values for *grayscale* and *RGB*. This results were according to previous works, where tissues morphologies of pork muscles from different origin were successfully characterized and classified using fractal information (Mendoza et al., 2009; Serrano et al., 2013).

Table 1. Fractal information and composition data blocks dependency study.

| | | | | Pork-loin | | | | | Salmon | | | | |
|---|---|---|---|---|---|---|---|---|---|---|---|---|---|
| | | | | *grayscale* | *R* | *G* | *B* | *RGB* | *grayscale* | *R* | *G* | *B* | *RGB* |
| *Complete spectra* | *Fd* | *Xw* | **Rcal** | 0.99 | 0.97 | 0.94 | 0.95 | 0.99 | 0.99 | 0.98 | 0.98 | 0.85 | 0.99 |
| | | | **RMSEcal** | 5E-04 | 6E-04 | 8E-04 | 6E-04 | 6E-04 | 5E-04 | 8E-04 | 7E-04 | 9E-03 | 6E-04 |
| | | | **Rval** | 0.96 | 0.95 | 0.91 | 0.92 | 0.98 | 0.95 | 0.95 | 0.92 | 0.75 | 0.95 |
| | | | **RMSEcv** | 3E-03 | 1E-03 | 3E-03 | 1E-03 | 1E-03 | 4E-03 | 3E-03 | 2E-03 | 9E-02 | 1E-03 |
| | | *Xf* | **Rcal** | 0.98 | 0.98 | 0.97 | 0.95 | 0.98 | 0.98 | 0.98 | 0.98 | 0.63 | 0.99 |
| | | | **RMSEcal** | 4E-04 | 4E-04 | 7E-04 | 6E-04 | 5E-04 | 4E-04 | 8E-04 | 6E-04 | 1E-01 | 5E-04 |
| | | | **Rval** | 0.95 | 0.95 | 0.95 | 0.93 | 0.95 | 0.94 | 0.94 | 0.94 | 0.60 | 0.94 |
| | | | **RMSEcv** | 2E-03 | 1E-03 | 2E-03 | 5E-04 | 4E-03 | 3E-03 | 3E-03 | 1E-03 | 1E-03 | 1E-03 |
| | *L* | *Xw* | **Rcal** | 0.98 | 0.97 | 0.95 | 0.95 | 0.98 | 0.98 | 0.98 | 0.98 | 0.74 | 0.98 |
| | | | **RMSEcal** | 5E-04 | 5E-04 | 8E-04 | 6E-04 | 6E-04 | 5E-04 | 8E-04 | 7E-04 | 9E-02 | 6E-04 |
| | | | **Rval** | 0.94 | 0.94 | 0.95 | 0.95 | 0.94 | 0.93 | 0.935 | 0.94 | 0.65 | 0.935 |
| | | | **RMSEcv** | 2E-03 | 1E-03 | 3E-03 | 8E-03 | 5E-03 | 4E-03 | 3E-03 | 2E-03 | 9E-01 | 5E-03 |
| | | *Xf* | **Rcal** | 0.98 | 0.98 | 0.96 | 0.95 | 0.98 | 0.98 | 0.98 | 0.98 | 0.78 | 0.98 |
| | | | **RMSEcal** | 4E-04 | 3E-04 | 7E-04 | 5E-04 | 5E-04 | 4E-04 | 7E-04 | 6E-04 | 9E-02 | 5E-04 |
| | | | **Rval** | 0.93 | 0.93 | 0.94 | 0.94 | 0.93 | 0.92 | 0.92 | 0.93 | 0.63 | 0.92 |
| | | | **RMSEcv** | 2E-03 | 2E-03 | 2E-03 | 2E-03 | 4E-03 | 3E-03 | 2E-03 | 5E-03 | 9E-01 | 4E-03 |

*Fd:* fractal dimension; *L*: lacunarity; *Xw:* water fraction; *Xf*: fat traction; $R^2$ *Cal*: calibration coefficient; *RMSEC*: root mean square error of calibration; $R^2$ *CV*: cross-validation coefficient; *RMSECV*: root mean square error of cross-validation; *R*: red channel of images; *G*: red channel of images; *B*: red channel of images; *RGB*: complete color information of image.

In order to evaluate the influence of the number of tones of the spectrum used in the prediction accuracy, with the aim to reducing the volume of processed data, the study was again done from one tone, such as in common image segmenting procedure, to complete spectrum. Data employed for each calculation was obtained isolating the fractal information from tones with the highest fractality (peaks on fractal spectra) from *grayscale* and *RGB*, and the improvement of the coefficients with the gradual inclusion of the contiguous tones was evaluated (10 contiguous tones were included in each step). Figure 6 shows the example of the evolution of *Rcal* and *Rval* between *Fd* and *Xf* following the progressive inclusion of tones in dependency analysis, both for *grayscale* (Figure 6A and C) and *RGB* (Figure 6B and D). Results describe how the inclusion of tones improved notably the coefficients and reduce the root mean square error (*RMSE)*. That effect was common for pork-loin (Figure 6A and B) and salmon (Figure 6C and D). Moreover, *RGB* presented less differences between coefficients obtained using only one tone and all tones, compared to grayscale. This effect was produced because the fact

that *RGB* starts with three tones from *R*, *G*, and *B* spectra peaks (one by channel), while *grayscale* had only one. These observations revealed that although the tone of spectra that form the peak collected the maximum information of sample morphology, the rest of tones represented fundamental information to explain in a high level, the variability produced by morphology of studied tissues.

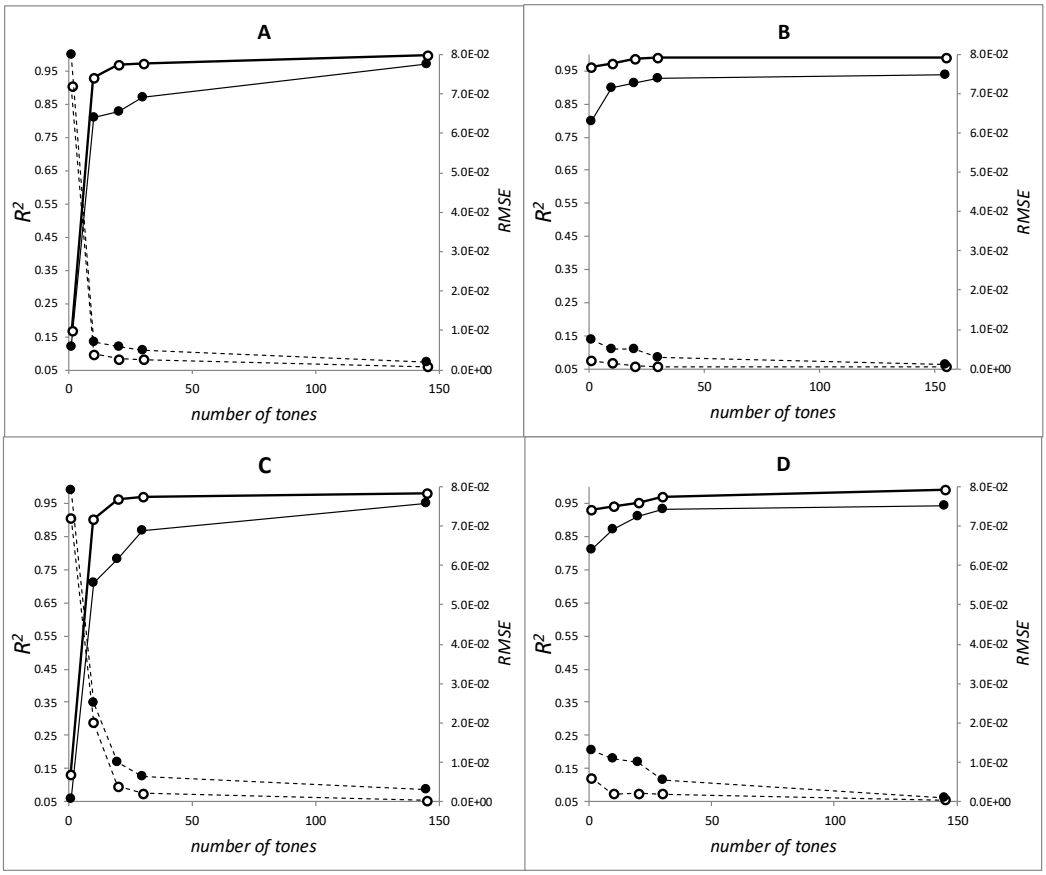


Figure 6. Evolution of regression coefficients between *Fd* (from grayscale and *RGB* data blocks) and *Xf* with number of tones included in study. Circumference: calibration; Dot: cross-validation; Black line: $R^2$; Dotted line: *RMSE*; A: Salmon *grayscale*; B: Salmon *RGB*; C: Pork-loin *grayscale*; D: Pork-loin *RGB.*

Therefore, the inclusion of information from complete color variability (*grayscale* and *RGB*) into study appeared to generate better results than each separate color channel (*R*, *G* and *B*), although it was a fact that the predominance of red tones, typical in these samples, allowed obtaining high coefficients for *R* isolated channel. It is known that *Xf* and *Xw* have a strong inverse relationship into the tissues systems as the studied here (Grau, Albarracín, Trinidad Pérez, Antequera, & Barat, 2011), then this feature also contributed to obtain those elevated coefficients and proves that this type of sliced products are susceptible to be inspected based on this type of non-destructive tools. As conclusion, fractal information based on both different parameters (*Fd* and *L*) and image types denoted high dependency from tissues features and natural morphology and then with their composition in terms of fat and water fraction.

## Conclusions

The capacity of fractal analytics on digital images had satisfactory results for characterizing the two different analyzed tissues. Fractal information collected the variability generated because the differences produced by the composition in terms of fat and water fraction for both pork-loin and salmon. In the same way, variability between pork-loin and salmon was also characterized because the differences in tissues morphology, mainly fat distribution within system, even in samples without differences in fat fraction. In regard to the two tested fractal parameters, both Fractal dimension and Lacunarity presented high dependency to fat and water fraction evolution, being both enough capable for characterize these properties of samples.

The type of image did not seem considerable differences in results, concluding as feasible to use whatever of their collect information. It was demonstrated that the

inclusion of tones reduce errors, being able to obtain high coefficients when all tones information was used. Overview, fractal analytics of images represent a simple, rapid and accessible non-destructive technique for characterizing the composition of tissues from different nature and complexity, which could complement processes of inspection with the aim of improve classification and selection operations within production chain.

**Bibliography**


Akar, E., Kara, S., Akdemir, H., & Kiriş, A. (2015). Fractal dimension analysis of cerebellum in Chiari Malformation type I. *Computers in Biology and Medicine*, *64*, 179–186. doi:10.1016/j.compbiomed.2015.06.024

Dowlati, M., Mohtasebi, S. S., Omid, M., Razavi, S. H., Jamzad, M., & De La Guardia, M. (2013). Freshness assessment of gilthead sea bream (Sparus aurata) by machine vision based on gill and eye color changes. *Journal of Food Engineering*, *119*, 277–287. doi:10.1016/j.jfoodeng.2013.05.023

Grau, R., Albarracín, W., Trinidad Pérez, M., Antequera, T., & Barat, J. M. (2011). Use of simultaneous brine thawing/salting in dry-cured Iberian ham production. *Journal of Food Engineering*, *104*(2), 316–321. doi:10.1016/j.jfoodeng.2010.12.023

He, Q., Zhu, L., Shen, Y., Lin, X., & Xiao, K. (2015). Evaluation of the effects of frozen storage on the microstructure of tilapia (Perciformes: Cichlidae) through fractal dimension method. *LWT - Food Science and Technology*, *64*(2), 1283–1288. doi:10.1016/j.lwt.2015.07.036

Ivorra, E., Verdu, S., Sánchez, A. J., Grau, R., & Barat, J. M. (2016). Predicting Gilthead Sea Bream (Sparus aurata) Freshness by a Novel Combined Technique of 3D Imaging and SW-NIR Spectral Analysis. *Sensors (Basel, Switzerland)*, *16*(10). doi:10.3390/s16101735

Jackman, P., Sun, D.-W., & Elmasry, G. (2012). Robust colour calibration of an imaging system using a colour space transform and advanced regression modelling. *Meat Science*, *91*(4), 402–7. doi:10.1016/j.meatsci.2012.02.014

Kesić, S., & Spasić, S. Z. (2016). Application of Higuchi's fractal dimension from basic to clinical neurophysiology: A review. *Computer Methods and Programs in Biomedicine*. doi:10.1016/j.cmpb.2016.05.014

Konda Naganathan, G., Cluff, K., Samal, A., Calkins, C. R., Jones, D. D., Lorenzen, C. L., & Subbiah, J. (2015). A prototype on-line AOTF hyperspectral image

acquisition system for tenderness assessment of beef carcasses. *Journal of Food Engineering*, *154*, 1–9. doi:10.1016/j.jfoodeng.2014.12.015

Lu, H., & Zheng, H. (2012). Fractal colour: A new approach for evaluation of acrylamide contents in biscuits. *Food Chemistry*, *134*, 2521–2525. doi:10.1016/j.foodchem.2012.04.085

Lu, H., Zheng, H., Hu, Y., Lou, H., & Kong, X. (2011). Bruise detection on red bayberry (Myrica rubra Sieb. & Zucc.) using fractal analysis and support vector machine. *Journal of Food Engineering*, *104*, 149–153. doi:10.1016/j.jfoodeng.2010.12.007

Mendoza, F., Valous, N. A., Allen, P., Kenny, T. A., Ward, P., & Sun, D. W. (2009). Analysis and classification of commercial ham slice images using directional fractal dimension features. *Meat Science*, *81*, 313–320. doi:10.1016/j.meatsci.2008.08.009

Mery, D., Lillo, I., Loebel, H., Riffo, V., Soto, A., Cipriano, A., & Aguilera, J. M. (2011). Automated fish bone detection using X-ray imaging. *Journal of Food Engineering*, *105*, 485–492. doi:10.1016/j.jfoodeng.2011.03.007

Quevedo, R., Ronceros, B., Garcia, K., Lopéz, P., & Pedreschi, F. (2011). Enzymatic browning in sliced and pur??ed avocado: A fractal kinetic study. *Journal of Food Engineering*, *105*, 210–215. doi:10.1016/j.jfoodeng.2011.02.012

Quevedo, R., Valencia, E., Cuevas, G., Ronceros, B., Pedreschi, F., & Bastías, J. M. (2013). Color changes in the surface of fresh cut meat: A fractal kinetic application. *Food Research International*, *54*, 1430–1436. doi:10.1016/j.foodres.2013.10.006

Ropodi, a. I., Panagou, E. Z., & Nychas, G.-J. E. (2016). Data mining derived from food analyses using non-invasive/non-destructive analytical techniques; determination of food authenticity, quality & safety in tandem with computer science disciplines. *Trends in Food Science & Technology*, *50*, 11–25. doi:10.1016/j.tifs.2016.01.011

Serrano, S., Perán, F., Jiménez-Hornero, F. J., & Gutiérrez de Ravé, E. (2013). Multifractal analysis application to the characterization of fatty infiltration in Iberian and White pork sirloins. *Meat Science*, *93*(3), 723–32. doi:10.1016/j.meatsci.2012.11.015

Torres, I. C., Amigo Rubio, J. M., & Ipsen, R. (2012). Using fractal image analysis to characterize microstructure of low-fat stirred yoghurt manufactured with microparticulated whey protein. *Journal of Food Engineering*, *109*(4), 721–729. doi:10.1016/j.jfoodeng.2011.11.016

Weissman, A., & Binah, O. (2014). The fractal nature of blood glucose fluctuations. *Journal of Diabetes and Its Complications*, *28*, 646–651. doi:10.1016/j.jdiacomp.2014.05.009

Zheng, H., Jiang, L., Lou, H., Hu, Y., Kong, X., & Lu, H. (2011). Application of artificial neural network (ANN) and partial least-squares regression (PLSR) to predict the changes of anthocyanins, ascorbic acid, Total phenols, flavonoids, and antioxidant activity during storage of red bayberry juice based on fractal ana. *Journal of Agricultural and Food Chemistry*, *59*(2), 592–600. doi:10.1021/jf1032476